Shear Dynamic Modulus of Nematic Elastomers: Modified Rouse Model

Vladimir P. Toshchevikov*,†,‡ and Yuli Ya. Gotlib†

Institute of Macromolecular Compounds, Russian Academy of Sciences, Bolshoi Prospect 31, V.O., Saint-Petersburg, 199004, Russia, and Leibniz Institute of Polymer Research Dresden, Hohe Strasse 6, Dresden, 01069, Germany

Received December 10, 2008; Revised Manuscript Received February 27, 2009

ABSTRACT: We develop a microscopic theory of dynamic mechanical properties of nematic elastomers taking the chain structure of network strands explicitly into account. We use an approach in which network strands are modeled as a sequence of Gaussian subchains, whose elasticity constants and friction coefficients are different for motions parallel and perpendicular to the LC-director: $K_{\|} \neq K_{\perp}$ and $\zeta_{\|} \neq \zeta_{\perp}$ (a modified Rouse model). We show that the dynamic modulus of an ordered nematic elastomer, $G^* = G' + iG''$, should demonstrate a frequency behavior very similar to that of usual (nonordered) rubbers; especially, it should display a frequency domain with a Rouse-like behavior, $G' \cong G'' \sim \omega^{1/2}$, a feature which is confirmed by experiments. In contrast to the usual rubbers, nematic elastomers are characterized by the anisotropy of the dynamic mechanical behavior with respect to the LC director, **n**. In agreement with experiment we show that for prolate systems in the D-geometry (when **n** is parallel to the shear velocity) G'_D greatly decreases around the nematic isotropic phase transition, whereas in the V-geometry (when **n** is perpendicular to the shear plane) G'_V does not demonstrate such a singularity. We discuss the predictions of our theory for other geometries under shear deformation.

1. Introduction

Liquid crystalline polymer networks containing rigid, rodlike mesogenic fragments in their strands form nematic elastomers. These materials combine in an unique way the long-chain elasticity of rubbers with the easy orientability of liquid crystals (LCs).[1−27] Remarkable properties of nematic elastomers are their ability to change their shape significantly around the nematic−isotropic (N−I) phase transition and their high sensitivity to weak external fields (electric, magnetic and mechanical). Due to their unique properties, nematic elastomers have a fascinating potential for technical applications (such as electro-optical display devices, piezoelectric and nonlinear optical systems, actuators, and artificial muscles).

The equilibrium properties of nematic elastomers (their phase transitions and their stress−strain relations) have been studied in detail.[1−11] At the same time, the dynamics of nematic elastomers have only recently entered the focus of much interest:[12−26] this is due, on the one hand, to the fact that it became possible to synthesize homogeneous (monodomain) nematic elastomers,[9,10,15,16,21−23] and on the other hand, to recent dynamic mechanical experiments which have been performed both for side-[15,16,21,22] and main-chain[23] monodomain nematic elastomers.

A monodomain nematic elastomer is characterized by the anisotropy of its dynamic mechanical properties: the response of an ordered sample to a periodic shear strain depends on the direction of the strain with respect to the LC director, **n**. In a typical dynamic mechanical experiment, one uses one of the three principal geometries, denoted by D (displacement), by V (vorticity) and by G (for **n** along the shear gradient),[14] see Figure 1. Each geometry provides a corresponding dependence of the complex dynamic modulus, G^* on frequency, ω, namely $G^*_D = G'_D + iG''_D$, $G^*_V = G'_V + iG''_V$, and $G^*_G = G'_G + iG''_G$. In recent dynamic mechanical experiments,[15,16,21−23] monodomain LC films were investigated with a planar orientation of the LC-director within the films; thus it was possible to conduct experiments only for the D- and the V-geometries. For all nematic elastomers investigated in refs.[15,16,21−23] the frequency dependent dynamic moduli, $G^*_D(\omega)$ and $G^*_V(\omega)$ were found to demonstrate two frequency regimes, both typical for usual rubbers: (i) a low frequency hydrodynamic regime ($G' = \text{const}$; $G'' \sim \omega$) at $\omega < \tau_E^{-1}$ and (ii) a viscoelastic regime which is characterized by a power law $G' \sim G'' \sim \omega^n$ at $\omega > \tau_E^{-1}$, where τ_E is the longest relaxation time of the network strands. Furthermore, all the side-chain nematic elastomers demonstrated a Rouse-like behavior in the viscoelastic regime, $G' \cong G'' \sim \omega^{0.5}$,[15,16,21,22] whereas the main-chain nematic elastomers deviated from the Rouse-like behavior: for the latter one found $G' \cong C_1\omega^n$ and $G'' \cong C_2\omega^n$ ($C_1 \neq C_2$), with the exponent n being less than 0.5 and being temperature-dependent.[23] This difference is related to the differences in the microstructures between the side- and the main-chain LC elastomers. The side-chain LC elastomers exhibit only isotropic and nematic phases,[15,16,21,22] whereas the main-chain ones exhibit additionally smectic C (SmC) phases and SmC domains in the nematic and isotropic phases.[23] The formation of SmC domains affects strongly the mechanical characteristics of the main-chain LC elastomers in both the nematic and the isotropic phases.[23]

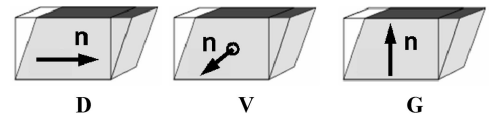

Figure 1. Three principal geometries of a simple shear experiment with three orientations of the nematic director **n**: D (displacement), V (vorticity), and G (for **n** along the shear gradient).

To treat the experimental data on the dynamic mechanical properties of nematic elastomers, one can use several theories.[2,12,14] All these theories use a continuum medium approach and are based on the coupling between the linear elasticity of a network in its hydrodynamic regime, $\omega\tau_E < 1$, and the independent rotations of the LC-director, see also the discussion.[16−20] Although existing continuum theories can explain

* Author to whom correspondence should be addressed. Telephone: 7-(812)-3285601. Fax: 7-(812)-3286869. E-mail: toshchevikov@imc.macro.ru.
† Institute of Macromolecular Compounds, Russian Academy of Sciences.
‡ Leibniz Institute of Polymer Research Dresden.

10.1021/ma802757g CCC: $40.75
Published on Web 04/16/2009

many experimental facts (e.g., the anisotropy of the dynamic mechanical properties of nematic elastomers, the reduction of G'_D as compared to G'_V, etc.), they are valid only in the hydrodynamic regime, $\omega\tau_E < 1$, and they do not make predictions in the viscoelastic regime, $\omega\tau_E > 1$, where the main effects are due to the chain dynamics of network strands. There are no microscopic theories in the literature which consider the effects of the chain dynamics on the mechanical relaxation of nematic elastomers.

In order to overcome these drawbacks, we put forward a microscopic theory of the dynamic mechanical properties of nematic elastomers using a network model which takes the chain structure of the network strands explicitly into account. We use an approach,[24−26,28−31] in which the fragments of polymer chains in the LC state are considered to move on the background of a static (immobile) LC director. For nematic elastomers the director relaxation time, τ_n, was found to be of the same order as the longest relaxation time of the network strands, $\tau_n \sim \tau_E \sim 10^{-2}$ s, e.g., see p 320 of ref 16. Therefore, in the viscoelastic regime, $\omega\tau_E > 1$, one can neglect the director rotations and use the assumption that the motions of the network strands occur on the background of an immobile LC director. The assumption of an immobile LC director has been used by many authors in describing the dynamics of LC polymer melts.[28−31] Recently,[24−26] this approach was applied by us in describing the relaxation spectrum of a main-chain nematic elastomer for intrachain motions with immobile network junctions.

In the present work, we extend our previous theories[24−26] and calculate the storage and loss moduli for the three principal geometries (D, V, G). We use here a modified Rouse model[32] which can be applied both for side- and main-chain LCs. We consider the mobility of network strands on scales larger than such chain fragments (subchains), whose statistics is Gaussian. The orientation ordering of mesogenic units results in the orientational anisotropy of both main- and side-chain network strands due to the covalent bonding of the mesogens to the chain backbones. Thus, each network strand is modeled here as a sequence of Gaussian subchains whose viscoelastic parameters are different for motions parallel and perpendicular to the LC director (a modified Rouse model). In general, such a model can describe the dynamics of both main- and side-chain anisotropic macromolecules. However, the existing main-chain LC elastomers exhibit layer-structured SmC domains in their nematic and isotropic phases, the effects of the SmC domains on the dynamics being rather strong. The modified Rouse model does not take into account the presence of such domains in the structure and represents thus a homogeneous chain; therefore, it can be immediately applied only for side-chain nematic elastomers, whose structure is homogeneous both in the isotropic and in the nematic phases. The extension of the theory to main-chain nematic elastomers requires the introduction of smectic domains in the network model, effects which are not discussed here and can be a topic for further generalizations.

The paper is organized as follows. In section 2, we present the physical basis for introducing the modified Rouse model to be used. In section 3, we derive analytical expressions for the components of the complex moduli (G^*_D, G^*_V, and G^*_G) using a rather arbitrary network structure built from anisotropic Rouse chains. In contrast to refs 24−26, we take into consideration not only the intrachain processes with immobile network junctions but also the interchain collective motions. We find the interconnection between the mechanical characteristics for an ordered nematic elastomer and for an isotropic network structure of the same topology. In section 4, we calculate the frequency and temperature dependences for the components of the complex moduli G^*_D, G^*_V and G^*_G using a regular cubic network model. We show that results of our theory for the D- and V-geometries are in a good agreement with experimental data on side-chain nematic elastomers.[15,16,21,22] We discuss the predictions of the theory for the G-geometry.

2. Modified Rouse Model for LC-Ordered Macromolecules

The physical concept which is the basis here for describing the viscoelastic properties of LC-ordered macromolecules is similar to the ideas of Rouse[33] for conventional (nonordered) polymers. The main idea is to consider the motion on scales larger than the Kuhn segment and to ignore the short-scale motions. This concept was used in ref 32 for LC polymer chains. As for isotropic chains,[33] we divide a polymer chain in the LC state into N equal subchains. Each subchain is a portion of a polymer chain just long enough, so that at equilibrium its end-to-end distribution is Gaussian. In contrast to nonordered macromolecules, which are characterized by isotropic end-to-end distributions, the shape of the subchains in an ordered state is anisotropic.[1−8] For main-chain macromolecules, the anisotropy of the shape of polymeric coils is caused by the orientation of the mesogenic fragments chemically incorporated into the chain's backbone. For side-chain macromolecules, the anisotropy of the mesogenic units in the side chains also leads to the anisotropy of the polymeric coils due to the covalent rigid bonding of the mesogens to the backbones.

Thus, both for main- and side-chain macromolecules, the probability of the end-to-end vector, $\mathbf{b}$, of a Gaussian subchain in LC state can be written as[5−8,32]

$$p(\mathbf{b}) = (2\pi l_0 L)^{-3/2}\left(\frac{l_0^3}{l_{||}l_{\perp}^2}\right)\exp\left[-\left(\frac{3b_{||}^2}{2l_{||}L} + \frac{3\mathbf{b}_{\perp}^2}{2l_{\perp}L}\right)\right] \quad (1)$$

where $b_{||}$ and $\mathbf{b}_{\perp}$ are the components of $\mathbf{b}$ parallel and perpendicular to the LC director; L is the contour length of the subchain; $l_{||}$ and $l_{\perp}$ are the persistence lengths parallel and perpendicular to the director, respectively. The values $l_{||}$ and $l_{\perp}$ are different from the value l_0 of the persistence length of the chain in the isotropic state and are functions of the nematic order parameter S, where

$$S = \left\langle \frac{3\cos^2\theta - 1}{2} \right\rangle \quad (2)$$

Here θ is the angle between a given orienting rod-like (mesogenic) unit and the LC director; $\langle ... \rangle$ means averaging over all the orienting units. The concrete form of the dependences $l_{||}(S)$ and $l_{\perp}(S)$ is determined by the internal structure of the subchains and by the connectivity of the orienting units to the chain backbones. To find the concrete dependences of $l_{||}(S)$ and $l_{\perp}(S)$ for different chain models (freely jointed-rods chain, elastically jointed-rods chain, worm-like chain, main-chain macromolecules with spacers, side-chain macromolecules, etc.), one can see the review.[8]

Now, the conformational distribution function of a Gaussian chain consisting of N such anisotropic subchains is given by

$$P(\{\mathbf{R}_n\}) = \prod_{n=1}^{N} p(\mathbf{R}_n - \mathbf{R}_{n-1}) = (2\pi l_0 L)^{-3N/2}\left(\frac{l_0^3}{l_{||}l_{\perp}^2}\right)^N \exp\left[-\left(\sum_{n=1}^{N}\frac{3(R_{||,n} - R_{||,n-1})^2}{2l_{||}L} + \sum_{n=1}^{N}\frac{3(\mathbf{R}_{\perp,n} - \mathbf{R}_{\perp,n-1})^2}{2l_{\perp}L}\right)\right] \quad (3)$$

where $\mathbf{R}_n$ are the coordinates of the ends of the subchains.

As for the Rouse model,[33] the anisotropic Gaussian chains used here can be represented by a mechanical model: the $(N+1)$ beads are considered to be connected by N harmonic springs.

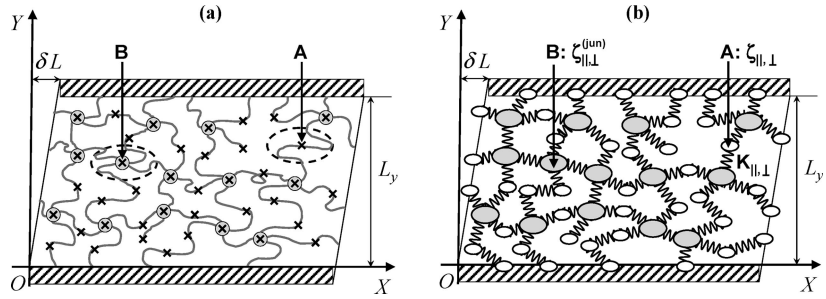

Figure 2. (a) Schematic sketch of a nematic elastomer under shear deformation. Cross-links are marked by filled circles; daggers show the dividing points of the network strands into subchains, see text for details. (b) Anisotropic Gaussian network model corresponding to a nematic elastomer presented in Figure 2a. Ellipsoidal beads denote diffusion anisotropy of the subchains inside network strands (white beads) and of the subchains attached to the cross-link points (filled beads).

Using eq 3, we can write the potential energy of an anisotropic Gaussian chain as follows:

$$U(\{\mathbf{R}_n\}) = \frac{1}{2}K_{\|}\sum_{n=1}^{N}(R_{\|,n} - R_{\|,n-1})^2 + \frac{1}{2}K_{\perp}\sum_{n=1}^{N}(\mathbf{R}_{\perp,n} - \mathbf{R}_{\perp,n-1})^2 \tag{4}$$

In contrast to the classical Rouse model, the harmonic springs in the LC state are anisotropic and characterized by two elasticity constants $K_{\|}$ and $K_{\perp}$ for the stretching of a subchain in directions parallel and perpendicular to the LC director. The elasticity constants are related to the principal persistence lengths, $l_{\|}(S)$ and $l_{\perp}(S)$; this relation follows from Equations 3 and 4:

$$K_{\alpha} = \frac{3kT}{l_{\alpha}L} \quad (\alpha = \|, \perp) \tag{5}$$

The diffusion mobility of the chain fragments in the LC state is known to be anisotropic.[34−37] To describe this effect we stipulate for each bead two friction coefficients, $\zeta_{\|}$ and $\zeta_{\perp}$, corresponding to translational motions parallel and perpendicular to the LC director. These frictions coefficients are functions of the order parameter: $\zeta_{\|} = \zeta_{\|}(S)$ and $\zeta_{\perp} = \zeta_{\perp}(S)$. In general, the evaluation of these dependences is a special problem[34−37] and will be discussed in section 4.

To sum up, we describe the dynamics of LC polymer chains by means of a modified Rouse model consisting of Gaussian subchains with anisotropic viscoelastic parameters: two elasticity constants, $K_{\|}$ and $K_{\perp}$, and two friction coefficients, $\zeta_{\|}$ and $\zeta_{\perp}$ (cf. with ref 32). Note that such Gaussian chains do not describe correctly the local structure of the macromolecules but they do describe correctly the *large-scale* dynamics of macromolecules of an arbitrary structure (main- and side-chain polymers, etc.), i.e. the model is universal in this sense. Note, however, that existing main-chain LC elastomers possess a heterogeneous domain structure with SmC domains. The chain model introduced here does not take into account such heterogeneities and, therefore, can not be applied to existing main-chain nematic elastomers. On the other hand, it can be immediately applied to the existing side-chain nematic elastomers which do not exhibit such heterogeneities.

The quantities $K_{\|}$, $K_{\perp}$, $\zeta_{\|}$, and $\zeta_{\perp}$ are the parameters of the model. In Section 4 we fix the dependences of $K_{\|}$, $K_{\perp}$, $\zeta_{\|}$, and $\zeta_{\perp}$ on the order parameter S using a freely jointed-ellipsoids chain. This will allow us to discuss the dependences of the principal dynamic moduli G_D^*, G_V^* and G_G^* on S.

3. Dynamic Modulus of a Generalized Network Structure Built from Anisotropic Rouse Chains

In this section we derive expressions for the principal dynamic moduli, G_D^*, G_V^* and G_G^* as functions of the parameters, $K_{\|}$, $K_{\perp}$, $\zeta_{\|}$, and $\zeta_{\perp}$ using a generalized network structure built from anisotropic Rouse chains. We build a network model as follows: each network strand of a LC elastomer (Figure 2a) is divided up into identical Gaussian subchains. In Figure 2a, the dividing points are marked by daggers and the network cross-links are denoted by filled circles. As a result, we obtain a network structure built from Gaussian subchains (Figure 2b). Each subchain is characterized by the viscoelastic parameters $K_{\|}$, $K_{\perp}$, $\zeta_{\|}$, and $\zeta_{\perp}$ (point A in Figure 2, parts a and b). The number of subchains in the strands between junctions can vary in general from chain to chain.

The friction coefficients of the jth junction, $\zeta_{j,\|}^{(jun)}$ and $\zeta_{j,\perp}^{(jun)}$, represent a sum of friction coefficients of subchains intersecting at a cross-link point (point B in Figure 2, parts a and b), i.e.:

$$\frac{\zeta_{j,\|}^{(jun)}}{\zeta_{\|}} = \frac{\zeta_{j,\perp}^{(jun)}}{\zeta_{\perp}} \equiv \gamma_j = \text{const} \tag{6}$$

where γ_j is the number of chains intersecting at the jth cross-link; γ_j is independent of S.

As a result, we have a network structure of a rather arbitrary topology (Figure 2b); the polydispersity of network strands, the multifunctionality of branching points and the presence of dangling chains are all taken into consideration. However, we do not discuss hydrodynamic and excluded volume effects as long as dense polymer systems display screening of both hydrodynamic and volume interactions (Flory's theorem).[38]

For a fixed network structure one can, of course, calculate the relaxation spectrum for motions parallel and perpendicular to the LC director. However, to derive expressions for the dynamic moduli of an anisotropic network structure is a special problem. In the literature, there are no molecular theories which provide expressions for the dynamic moduli for anisotropic networks taking the chain structure of the network strands explicitly into account. Below, we present such derivation.

We follow a standard method described, e.g., by Doi and Edwards[38] for isotropic systems. As in ref 38, we consider an infinitesimal periodic shear deformation applied along the x-axis to a sample, Figure 2b. This leads to the shear flow[38]

$$\mathrm{v}_x(\mathbf{R}, t) = \kappa(t)R_y, \quad \mathrm{v}_y = \mathrm{v}_z = 0 \tag{7}$$

where $\mathbf{v}(\mathbf{R},t) = (\mathrm{v}_x,\mathrm{v}_y,\mathrm{v}_z)$ is the *macroscopic* velocity field at the point $\mathbf{R} = (\mathrm{R}_x,\mathrm{R}_y,\mathrm{R}_z)$ and $\kappa(t)$ is the shear rate which is related to the shear displacement $\delta L(t)$ as follows,[38] see Figure 2b:

$$\kappa(t) = \frac{\mathrm{d}}{\mathrm{d}t}\frac{\delta L(t)}{L_y} \tag{8}$$

Here L_y is the dimension of a sample along the y-direction. We consider geometries when the LC-director $\mathbf{n}$ lies along one of

the axes x, y, or z of the shear flow. Note that the *macroscopic* velocity field $\mathbf{v}(\mathbf{R},t)$ represents an average of the *microscopic* one.[38] This means that the velocity of a given bead, $\dot{\mathbf{R}}_I$, is related to its average position $\langle \mathbf{R}_I \rangle$ as follows:

$$\langle \dot{\mathbf{R}}_I \rangle = \mathbf{v}(\langle \mathbf{R}_I \rangle, t) \tag{9}$$

Here the averaging goes over the statistical ensemble, and the index I runs over all the beads.

The shear deformation results in the appearance of the mechanical stress, σ_{xy}. If the shear rate $\kappa(t)$ is small enough, the shear stress depends linearly on $\kappa(t)$ and can be written as[38]

$$\sigma_{xy}(t) = \int_{-\infty}^{t} \mathrm{d}t'\, G_{xy}(t - t')\kappa(t') \tag{10}$$

where $G_{xy}(t)$ is the shear relaxation modulus. For anisotropic systems the relaxation modulus can depend on the geometry of the shear with respect to the director $\mathbf{n}$; therefore, we introduce an index xy for $G_{xy}(t)$. Now, our aim is to calculate the stress $\sigma_{xy}(t)$ in an anisotropic network structure for a given history of the macroscopic velocity gradient, $\kappa(t)$. Obtaining $\sigma_{xy}(t)$ in the form of eq 10, we derive the expression for the relaxation modulus $G_{xy}(t)$.

We start from a microscopic expression for the mechanical stress tensor, σ_{xy}:[38]

$$\sigma_{xy} = -\frac{1}{V}\sum_I \langle F_{x,I} R_{y,I} \rangle \tag{11}$$

where V is the volume of the system, $R_{y,I}$ is the y-component of the Ith bead and $F_{x,I}$ is the x-component of the force acting on it. The force $F_{x,I}$ includes the contribution of the Brownian force $F_{x,I}^{(\mathrm{Br})}$ and of the elastic force $F_{x,I}^{(\mathrm{El})} \equiv -\partial U/\partial R_{x,I}$; it can be written as follows:[38]

$$F_{x,I} = F_{x,I}^{(\mathrm{Br})} - K_x \sum_J \mathbf{A}_{IJ} R_{x,J} \tag{12}$$

where $\mathbf{A} = (A_{IJ})$ is the connectivity matrix, see refs.[39−45] for details. The nondiagonal element A_{IJ} of $\mathbf{A}$ equals -1 if the Ith and Jth beads are connected and is 0 otherwise; the diagonal element A_{II} of $\mathbf{A}$ equals the number of bonds emanating from the Ith bead. Inserting eq 12 into eq 11 and using $\langle F_x^{(Br)} R_y \rangle = 0$, we have the following for $\sigma_{xy}(t)$:

$$\sigma_{xy} = \frac{K_x}{V}\sum_{I,J} \mathbf{A}_{IJ} \langle R_{x,J} R_{y,I} \rangle \tag{13}$$

Equation 13 contains two contributions: (i) from the beads which are inside the network and (ii) from the beads which are fixed on the plate (Figure 2b). The equation of motion for the beads inside the network represents a balance between elastic, Brownian, and viscous forces and, according to the Lagrange equation, is written as follows:[38−45]

$$\zeta_{\alpha,i}[\dot{R}_{\alpha,i} - \mathrm{v}_\alpha(t, \mathbf{R}_i)] + K_\alpha \sum_J \mathbf{A}_{iJ} R_{\alpha,J}(t) = F_{\alpha,i}^{(\mathrm{Br})}(t) \tag{14}$$

Here and in the following we will view small indices (i, j,...) as running over beads inside the network, small indices with primes (i', j',...) as running over beads at the plate and large ones (I, J,...) as running over all the beads both inside the network and at the plate. The position of each bead, $\mathbf{R}_I$, is determined by its average value, $\langle \mathbf{R}_I(t) \rangle$, which follows the macroscopic velocity field, and by the fluctuating displacements, $\delta\mathbf{R}_I$, from the average value:

$$\mathbf{R}_I(t) = \langle \mathbf{R}_I(t) \rangle + \delta\mathbf{R}_I(t) \tag{15}$$

Inserting Equation 15 into eq 13 we can rewrite σ_{xy} as follows

$$\sigma_{xy} = \sigma_{xy}^{(1)} + \sigma_{xy}^{(2)} \tag{16}$$

where

$$\sigma_{xy}^{(1)} = \frac{K_x}{V}\sum_{I,J} \mathbf{A}_{IJ} \langle R_{x,J} \rangle \langle R_{y,I} \rangle \tag{17}$$

$$\sigma_{xy}^{(2)} = \frac{K_x}{V}\sum_{I,J} \mathbf{A}_{IJ} \langle \delta R_{x,J} \delta R_{y,I} \rangle \tag{18}$$

Let us consider, first, the contribution $\sigma_{xy}^{(1)}$. The positions of beads at the plate are fixed on the plate, so that $\mathbf{R}_{i'}(t) \equiv \langle \mathbf{R}_{i'}(t) \rangle$. The average positions of the beads inside the network can be obtained from eq 14. Averaging eq 14 and using eq 9 we have

$$K_\alpha \sum_J \mathbf{A}_{iJ} \langle R_{\alpha,J}(t) \rangle = 0 \tag{19}$$

Thus, the sum over an index I in eq 17 for $\sigma_{xy}^{(1)}$ contains only the terms from the beads at the plate ($I = i'$) since the terms from internal beads ($I = i$) equal zero according to eq 19. Using this fact and taking into account the equality $\langle R_{y,i'} \rangle = L_y$ for the beads at the plate we can rewrite eq 17 as

$$\sigma_{xy}^{(1)} = \frac{L_y K_x}{V}\sum_{i',J} \mathbf{A}_{i'J} \langle R_{x,J} \rangle \tag{20}$$

or

$$\sigma_{xy}^{(1)} = \frac{1}{\Xi}\sum_{i'} F_{x,i'} \tag{21}$$

where $\Xi = V/L_y$ is the area of the plate and $F_{x,i'}$ is the force acting on the i'th bead due to the other beads. Here lies the physical meaning of the quantity $\sigma_{xy}^{(1)}$. As follows from eq 21, $\sigma_{xy}^{(1)}$ is the stress appearing on the plate when the beads inside the network are at the positions $\langle \mathbf{R}_I \rangle$ which correspond to their *static* state according to Equation 19. Thus, $\sigma_{xy}^{(1)}$ is the *static* or *equilibrium* stress of the network. Thus, for $\sigma_{xy}^{(1)}$ we can write for small δL:

$$\sigma_{xy}^{(1)} = G_{xy}^{(\mathrm{eq})} \frac{\delta L(t)}{L_y} \tag{22}$$

where $G_{xy}^{(\mathrm{eq})}$ is the equilibrium modulus of the network for a given xy-geometry. Note that the equilibrium stress appears due to the real connections between the network fragments and the plate. If such connections are absent ($A_{i'I} = 0$) all terms on the right-hand side of eq 20 are zero and $\sigma_{xy}^{(1)} = 0$. For example, it is well-known that the equilibrium stress does not manifest itself in dynamic mechanical experiments for polymer melts and solutions,[38,46] but it does for bulk elastomers;[46,47] see also the experiments for nematic elastomers.[15,16,21−23]

For Gaussian structures, it is possible to relate the equilibrium modulus of the anisotropic network ($G_{xy}^{(\mathrm{eq})}$) to that of the isotropic network structure (G_0) which has the same connectivity as a nematic network. For usual (nonordered) rubbers, one has[46]

$$G_0 = \nu kT \tag{23}$$

where ν is the number of chains in the unit volume. In order to relate $G_{xy}^{(\mathrm{eq})}$ and G_0 we note that when applying a static shear along the x-direction to a network, only the x-projections of

the network strands change and the y, z - projections stay unchanged. It means that the total force appearing at the plate, $F_x = \sum_{i'} F_{x,i'}$, should be directly proportional to the elasticity constant K_x. Subchains in an isotropic network are characterized by an elasticity constant K_0 which differs from the elasticity constants of the subchains in an anisotropic network ($K_{||} \neq K_0$, $K_{\perp} \neq K_0$); K_0 is related to the persistence length l_0 of isotropic chains:

$$K_0 = 3kT/l_0 L \tag{24}$$

Using the proportionality between F_x and K_x we have

$$F_x = F_x^{(0)} \frac{K_x}{K_0} \tag{25}$$

where F_x and $F_x^{(0)}$ are the forces appearing at the plates of anisotropic and isotropic networks of the same topology and at the same shear displacement δL.

Note that a nematic elastomer can stretch along the LC director during ordering,[2−8,16,22] so that its dimensions along the x, y, and z axes (L_x, L_y, L_z) can differ from those for the elastomer in the isotropic state ($L_x^{(0)}$, $L_y^{(0)}$ and $L_z^{(0)}$): $L_x = e_x L_x^{(0)}$, $L_y = e_y L_y^{(0)}$ and $L_z = e_z L_z^{(0)}$. Here e_x, e_y and e_z are the elongation ratios of the sample along the x, y and z-axes which should satisfy the condition of constant volume ($V \equiv L_y \cdot \Xi = \text{const}$): $e_x e_y e_z = 1$. Using the condition, $V \equiv L_y \cdot \Xi = \text{const}$ we have from eqs 21 and 22: $F_x = VG_{xy}^{(\text{eq})} \delta L / L_y^2$ and $F_x^{(0)} = VG_0 \delta L / (L_y^{(0)})^2$. Substituting the last two equations into eq 25, we obtain $VG_{xy}^{(\text{eq})} \delta L / L_y^2 = [K_x/K_0] \cdot VG_0 \delta L / (L_y^{(0)})^2$; this gives with eq 23

$$G_{xy}^{(\text{eq})} = \nu kT e_y^{\,2} l_0 / l_x \tag{26}$$

Here we have used the relations between the elasticity constants and the persistence lengths, eqs 5, and 24.

We now turn to the second contribution to the stress, $\sigma_{xy}^{(2)}$, which is given by eq 18. Note that the sum over the indices I and J in eq 18 contains only terms from the internal beads, $\langle \delta R_{x,j} \delta R_{y,i} \rangle$, as long as the beads at the plate are fixed on the plate, so that $\delta \mathbf{R}_{i'}(t) = 0$. The dynamic equation for $\delta R_{x,j}$ can be derived by subtracting eq 19 from 14. Doing this and taking into account eqs 7, 9, and 15 we obtain

$$\zeta_{\alpha,i} \delta \dot{R}_{\alpha,i} + K_\alpha \sum_j \mathbf{A}_{ij} \delta R_{\alpha,j}(t) = F_{\alpha,i}^{(\text{Br})}(t) + \delta_{\alpha x} \zeta_{\alpha,i} \kappa(t) \delta R_{y,i} \tag{27}$$

Here $\delta_{\alpha\beta}$ is the Kroneker delta. Note that due to the equality $\delta \mathbf{R}_{i'}(t) = 0$ the dynamics of the internal beads is now determined only by themselves and does not depend on the beads at the plate. It is convenient to rewrite eq 27 in matrix form. Dividing eq 27 by the friction coefficient of a spacer bead, ζ_α, we have

$$\hat{\mathbf{Z}} \frac{d}{dt} \{\mathbf{R}_\alpha\} + \frac{1}{\tau_\alpha^{(0)}} \hat{\mathbf{A}} \{\mathbf{R}_\alpha\} = \zeta_\alpha^{-1} \{\mathbf{F}_\alpha^{(\text{Br})}\} + \hat{\mathbf{Z}} \{\mathbf{R}_y\} \kappa(t) \delta_{\alpha x} \tag{28}$$

Here we have introduced the subvectors $\{\mathbf{R}_\alpha\} = \{\delta R_{\alpha,1}, \delta R_{\alpha,2}, ...\}^+$ and $\{\mathbf{F}_\alpha^{(\text{Br})}\} = \{F_{\alpha,1}^{(\text{Br})}, F_{\alpha,2}^{(\text{Br})}, ...\}^+$, and denoted by $\tau_\alpha^{(0)}$ a characteristic relaxation time of a single subchain in the α-projection:

$$\tau_\alpha^{(0)} = \frac{\zeta_\alpha}{K_\alpha} \tag{29}$$

According to assumption (6), the matrix $\hat{\mathbf{Z}}$ has a diagonal form: $Z_{ii} = 1$ if the ith bead is a spacer bead and $Z_{ii} = \gamma_i$ if the ith bead is a network junction. γ_i is the number of chains intersecting at the ith junction. Now, we introduce new coordinates, $\{\mathbf{r}_\alpha\}$:

$$\{\mathbf{r}_\alpha\} = \hat{\mathbf{Z}}^{1/2} \{\mathbf{R}_\alpha\} \tag{30}$$

Multiplying eq 28 with the matrix $\mathbf{Z}^{-1/2}$ we obtain

$$\frac{d}{dt}\{\mathbf{r}_\alpha\} + \frac{1}{\tau_\alpha^{(0)}} \hat{\mathbf{Z}}^{-1/2} \hat{\mathbf{A}} \hat{\mathbf{Z}}^{-1/2} \{\mathbf{r}_\alpha\} = \zeta_\alpha^{-1} \hat{\mathbf{Z}}^{-1/2} \{\mathbf{F}_\alpha^{(\text{Br})}\} + \{\mathbf{r}_y\} \kappa(t) \delta_{\alpha x} \tag{31}$$

Note that the matrix $\mathbf{Z}^{-1/2} \mathbf{A} \mathbf{Z}^{-1/2}$ is symmetric and, therefore, it has a unitary transform, $\mathbf{V}$

$$\hat{\mathbf{V}}^{-1} = \hat{\mathbf{V}}^+ \tag{32}$$

which diagonalizes it:

$$\hat{\mathbf{V}}^{-1} (\hat{\mathbf{Z}}^{-1/2} \hat{\mathbf{A}} \hat{\mathbf{Z}}^{-1/2}) \hat{\mathbf{V}} = \hat{\Lambda} \tag{33}$$

Here the diagonal matrix $\hat{\mathbf{\Lambda}} = \text{diag}(\lambda_1, \lambda_2, ...)$ contains the eigenvalues of the matrix $\hat{\mathbf{Z}}^{-1/2} \hat{\mathbf{A}} \hat{\mathbf{Z}}^{-1/2}$. Using the transformation $\hat{\mathbf{V}}$, we introduce now the normal coordinates, $\{\mathbf{q}_\alpha\}$:

$$\{\mathbf{q}_\alpha\} = \hat{\mathbf{V}}^{-1} \{\mathbf{r}_\alpha\} \tag{34}$$

Multiplying eq 31 by the matrix $\hat{\mathbf{V}}^{-1}$ we obtain a system of independent equations (with respect to the different values of the index, p),

$$\frac{d}{dt} q_{\alpha,p} + \tau_{\alpha,p}^{-1} q_{\alpha,p} = \zeta_\alpha^{-1} (\hat{\mathbf{V}}^{-1} \hat{\mathbf{Z}}^{-1/2} \{\mathbf{F}_\alpha^{(\text{Br})}\})_p + q_{y,p} \kappa(t) \delta_{\alpha x} \tag{35}$$

Here the relaxation times, $\tau_{\alpha,p}$, are determined through the eigenvalues λ_p as follows:

$$\tau_{\alpha,p} = \tau_\alpha^{(0)} / \lambda_p \tag{36}$$

Note that the values λ_p equal the eigenvalues for an isotropic network of the same topology as the nematic network. Therefore, the relaxation spectrum of an anisotropic network can be simply calculated using the results of previous theories[39−45] for isotropic networks, while taking further into account that the elementary relaxation times, $\tau_\alpha^{(0)}$, consist of two components, $\alpha = ||, \perp$.

Now, using the transform from $\{\mathbf{R}_\alpha\}$ to $\{\mathbf{q}_\alpha\}$ given by eqs 30 and 34, we can rewrite the expression for the stress tensor $\sigma_{xy}^{(2)}$ (eq 18) as follows

$$\sigma_{xy}^{(2)} \frac{V}{K_x} = \langle \{\mathbf{R}_y\}^+ \hat{\mathbf{A}} \{\mathbf{R}_x\} \rangle = \langle \{\mathbf{q}_y\}^+ \hat{\mathbf{V}}^+ \hat{\mathbf{Z}}^{-1/2} \hat{\mathbf{A}} \hat{\mathbf{Z}}^{-1/2} \hat{\mathbf{V}} \{\mathbf{q}_x\} \rangle = \langle \{\mathbf{q}_y\}^+ \hat{\Lambda} \{\mathbf{q}_x\} \rangle = \sum_p \lambda_p \langle q_{x,p} q_{y,p} \rangle \tag{37}$$

Here we have used the relations for the matrix $\mathbf{V}$ given by eqs 32 and 33. To obtain an expression for $\langle q_{x,p} q_{y,p} \rangle$ let us rewrite eq 35 for $\alpha = x$ and $\alpha = y$ separately:

$$\frac{d}{dt} q_{x,p} + \tau_{x,p}^{-1} q_{x,p} = \zeta_x^{-1} (\hat{\mathbf{V}}^{-1} \hat{\mathbf{Z}}^{-1/2} \{\mathbf{F}_x^{(\text{Br})}\})_p + q_{y,p} \kappa(t) \tag{38}$$

$$\frac{d}{dt} q_{y,p} + \tau_{y,p}^{-1} q_{y,p} = \zeta_y^{-1} (\hat{\mathbf{V}}^{-1} \hat{\mathbf{Z}}^{-1/2} \{\mathbf{F}_y^{(\text{Br})}\})_p \tag{39}$$

Now, multiplying eqs 38 and 39 with $q_{y,p}$ and $q_{x,p}$, respectively, summing these equations, and averaging with respect to the nonequilibrium distribution function, we obtain

$$\frac{\mathrm{d}}{\mathrm{d}t}\langle q_{x,p}q_{y,p}\rangle + [\tau_{x,p}{}^{-1} + \tau_{y,p}{}^{-1}]\langle q_{x,p}q_{y,p}\rangle = \langle q_{y,p}{}^2\rangle\kappa(t) \quad (40)$$

Here we have used $\langle F_x q_y\rangle = \langle F_y q_x\rangle = 0$. The solution of eq 40 can be written as[38]

$$\langle q_{x,p}q_{y,p}\rangle = \int_{-\infty}^{t} \mathrm{d}t' \exp[-(\tau_{x,p}{}^{-1} + \tau_{y,p}{}^{-1})(t - t')]\kappa(t')\langle q_{y,p}{}^2\rangle \quad (41)$$

In the framework of linear-response theory, when one looks for the first term of σ_{xy} in the series of infinitesimal $\kappa(t)$, one can replace the time-dependent value $\langle q_{y,p}{}^2\rangle$ in eq 41 by its equilibrium value $\langle q_{y,p}{}^2\rangle_{\mathrm{eq}}$.[38]

Note, however, that nematic elastomers are known to demonstrate a very interesting nonlinear stress−strain behavior[1−8] which can be observed also in dynamic mechanical experiments at $\delta L/L_y > > 10^{-4}$, see ref 18. In order to consider nonlinear effects one needs to solve eq 40 exactly. This equation contains a time-dependent factor $\langle q_{y,p}{}^2\rangle$ on the right-hand side. Moreover, high shear strains can change the instantaneous value of the order parameter, S, which now becomes time-dependent: $S = S(t)$. Therefore, the coefficients $\tau_{\alpha,p}$ on the left-hand side of eq 40 become time-dependent at high shear, since $\tau_{\alpha,p} \propto \zeta_\alpha(S)/K_\alpha(S)$. As a result, one obtains a nonlinear dynamic equation similar to eq 40 but with the time-dependent coefficients on both sides of the equation.

Although nonlinear effects can be incorporated into our model as shown above, their consideration is out of the scope of the present work and may be a topic of further investigation. Here we deal with the linear-response approximation where we replace the time-dependent factor $\langle q_{y,p}^2\rangle$ in eq 41 by its equilibrium value $\langle q_{y,p}{}^2\rangle_{\mathrm{eq}}$ as in ref 38.

Now, multiplying eq 39 by $q_{y,p}$, averaging with respect to the *equilibrium* distribution function and discarding the time derivative for *equilibrium* quantities we obtain for $\langle q_{y,p}{}^2\rangle_{\mathrm{eq}}$,

$$\begin{aligned}\langle q_{y,p}{}^2\rangle_{\mathrm{eq}} &= \tau_{y,p}\zeta_y{}^{-1}\langle(\hat{\mathbf{V}}^{-1}\hat{\mathbf{Z}}^{-1/2}\{\mathbf{F}_y^{(\mathrm{Br})}\})_p q_{y,p}\rangle_{\mathrm{eq}}\\ &= \frac{1}{\lambda_p K_y}\sum_{jk}(\hat{\mathbf{V}}^{-1}\hat{\mathbf{Z}}^{-1/2})_{pk}(\hat{\mathbf{V}}^{-1}\hat{\mathbf{Z}}^{1/2})_{pj}\langle F_{y,k}^{(\mathrm{Br})}R_{y,j}\rangle_{\mathrm{eq}}\\ &= \frac{1}{\lambda_p K_y}\sum_{j}(\hat{\mathbf{V}}^{-1}\hat{\mathbf{Z}}^{-1/2})_{pj}(\hat{\mathbf{V}}^{-1}\hat{\mathbf{Z}}^{1/2})_{pj}kT\\ &= \frac{kT}{\lambda_p K_y}(\hat{\mathbf{V}}^{-1}\hat{\mathbf{Z}}^{-1/2}\hat{\mathbf{Z}}^{1/2}(\hat{\mathbf{V}}^{-1})^{+})_{pp}\\ &= \frac{kT}{\lambda_p K_y}\end{aligned} \quad (42)$$

Here we have used the relation for the stochastic force, $\langle F_{y,k}^{(\mathrm{Br})}R_{y,j}\rangle_{\mathrm{eq}} = kT\delta_{jk}$,[38] and eq 32 for the matrix $\mathbf{V}$. Now, substituting eq 42 into eq 41 and using eq 37 we have for the stress component $\sigma_{xy}^{(2)}$:

$$\sigma_{xy}^{(2)} = \frac{kT}{V}\frac{K_x}{K_y}\sum_p \int_{-\infty}^{t}\mathrm{d}t'\exp[-(\tau_{x,p}{}^{-1} + \tau_{y,p}{}^{-1})(t - t')]\kappa(t') \quad (43)$$

Comparing the last expression with eq 10 and taking the contribution of the equilibrium modulus into account (eqs 16 and 22), we obtain for the modulus of a nematic network

$$G_{xy}(t) = G_{xy}^{(\mathrm{eq})} + \frac{kT}{V}\frac{K_x}{K_y}\sum_p \exp[-(\tau_{x,p}{}^{-1} + \tau_{y,p}{}^{-1})t] \quad (44)$$

This is a key result of our theory. Note that in the isotropic state (when $K_x = K_y$ and $\tau_{x,p} = \tau_{y,p} \equiv \tau_p$) the last expression reduces to a well-known expression for the relaxation modulus derived earlier for isotropic polymer systems.[38−45] The factor $2\tau_p{}^{-1}t$ in the exponent which is usual for isotropic systems[38−45] splits for an anisotropic system into two components, $(\tau_{x,p}{}^{-1} + \tau_{y,p}{}^{-1})t$, while an additional prefactor, K_x/K_y, appears.

Now, using eqs 36, one can rewrite eq 44 in terms of the eigenvalues λ_p of an isotropic network which has the same topology as the nematic network. We have

$$G_{xy}(t) = G_{xy}^{(\mathrm{eq})} + \frac{kT}{V}\frac{l_y}{l_x}\sum_p \exp[-2\lambda_p t/\tau_{xy}^{(0)}] \quad (45)$$

where $\tau_{xy}^{(0)}$ is now the elementary relaxation time for the given xy-geometry, which is related to the elementary relaxation times $\tau_x^{(0)}$ and $\tau_y^{(0)}$ in the x and y projections by

$$\frac{1}{\tau_{xy}^{(0)}} = \frac{1}{2}\left[\frac{1}{\tau_x^{(0)}} + \frac{1}{\tau_y^{(0)}}\right] \quad (46)$$

In eq 45, l_x and l_y are the persistence lengths of the subchain along the x and y axes; here we have used the relations between l_α and K_α ($\alpha = x,y$), given by eq 5.

Equation 45 reflects a very important and general result. One can see that the relaxation factor in $G_{xy}(t)$, which contains the time variable t, is determined for an anisotropic network by the sum of exponents only over the eigenvalues of the corresponding isotropic system, λ_p. This means that all features of the dynamic mechanical behavior for nematic elastomers should be similar to those of the usual (nonordered) rubbers. By this, we extend the results of previous theories for isotropic networks[39−45] to anisotropic systems. For instance, as for isotropic networks,[39−45] the relaxation modulus for nematic elastomers should demonstrate Rouse-like behavior $G_{xy}(t) \sim t^{-1/2}$ at $t < \tau_E$ due to the intrachain relaxation processes, while in the time domain $t > \tau_E$ it is determined by the interchain collective motions, and $G_{xy}(t) \sim t^{-3/2}$.[39,40,43,45] Here τ_E is the longest relaxation time of network strands. Furthermore, the polydispersity of network strands should result in the appearance of a stretched-exponential time dependence, $G_{xy}(t) \sim \exp[-(t/\tau_*)^\alpha]$ at $t > \tau_E(\bar{L})$, with the index α depending on the distribution function of chain lengths.[41,43] Here $\tau_E(\bar{L})$ is the longest relaxation time of the Rouse modes for a network strand of average contour length.

These findings can be reformulated also for the dynamic (complex) modulus, $G_{xy}^* = G'_{xy} + iG''_{xy}$:

$$G_{xy}^*(\omega) = i\omega\int_0^\infty G_{xy}(t)\mathrm{e}^{-i\omega t}\,\mathrm{d}t \quad (47)$$

Here, the real (G'_{xy}) and the purely imaginary (G''_{xy}) parts are the storage and the loss moduli, respectively. Inserting eq 45 into eq 47, we have for the (complex) dynamic modulus:

$$G_{xy}^*(\omega) = G_{xy}^{(\mathrm{eq})} + \frac{kT}{V}\frac{l_y}{l_x}\sum_p \frac{(\tau_{xy}^{(0)}\omega)^2 + 2i\lambda_p\tau_{xy}^{(0)}\omega}{(2\lambda_p)^2 + (\tau_{xy}^{(0)}\omega)^2} \quad (48)$$

We emphasize that the similarity of the dynamic mechanical behavior of nematic elastomers to that of usual rubbers, especially, the presence of a frequency domain with Rouse-like behavior, $G'_{xy}(\omega) \cong G''_{xy}(\omega) \sim \omega^{1/2}$, was pioneered and discussed in experimental works.[15,16,21,22] Thus, the above-found general results of our theory are unambiguously confirmed by experiment.

The main difference between the dynamic mechanical behaviors of nematic elastomers and of usual rubbers consists in the mechanical anisotropy of ordered nematic elastomers relative to the LC-director, **n**. This fact was clearly demonstrated experimentally[15,16,21−23] by measuring the dynamic modulus for the D- and V-geometries. This fact follows also from our theory.

Equation 45 gives the expressions for the principal relaxation moduli, $G_D(t)$, $G_G(t)$, and $G_V(t)$ which correspond to geometries in which **n** lies along the axes *x*, *y*, and *z*, respectively. Using eq 26 for the equilibrium modulus, $G_{xy}^{(eq)}$, we have for $G_D(t)$, $G_V(t)$, and $G_G(t)$:

$$G_D(t) = \nu kT e_\perp^2 \frac{l_0}{l_\parallel} + \frac{kT}{V}\frac{l_\perp}{l_\parallel}\sum_p \exp[-2\lambda_p t/\tau_D^{(0)}] \quad (49a)$$

$$G_V(t) = \nu kT e_\perp^2 \frac{l_0}{l_\perp} + \frac{kT}{V}\sum_p \exp[-2\lambda_p t/\tau_V^{(0)}] \quad (49b)$$

$$G_G(t) = \nu kT e_\parallel^2 \frac{l_0}{l_\perp} + \frac{kT}{V}\frac{l_\parallel}{l_\perp}\sum_p \exp[-2\lambda_p t/\tau_G^{(0)}] \quad (49c)$$

Here the elementary relaxation times for D, V, and G geometries have the following form:

$$\tau_D^{(0)} = \tau_G^{(0)} = 2[(\tau_\parallel^{(0)})^{-1} + (\tau_\perp^{(0)})^{-1}]^{-1} \quad \text{and} \quad \tau_V^{(0)} = \tau_\perp^{(0)} \quad (50)$$

We remind that in eqs 49a−49c, e_α are the elongation ratios of the sample along the director ($e_\parallel$) and perpendicular to it ($e_\perp$). Two types of experiments are possible. In one case,[15,16,21,22] the sample is placed between two hard plates and remains unstretched during ordering ($e_\parallel = e_\perp = 1$). The LC order in this case appears due to the reorientation of the chain fragments at the fixed sample boundaries. In another possible case,[22] the boundaries of the sample are free and the sample can change its shape during ordering ($e_\parallel \neq 1$ and $e_\perp \neq 1$).

From eqs 49a−49c, general relations between the principal moduli follow. In general, depending on the chemical architecture of nematically ordered mesogenic groups inside the polymer chains, the conformations of the polymer coils may be prolate ($l_\parallel > l_\perp$) or oblate ($l_\parallel < l_\perp$).[5−9] For a prolate sample ($l_\parallel > l_\perp$) we have the following inequalities: $G_D < G_V < G_G$, which hold both for unstretched ($e_\parallel = e_\perp = 1$) and for stretched ($e_\perp < 1 < e_\parallel$) samples, see eqs 49a−49c. Note that the inequality $G_D < G_V$ was also found experimentally[15,16,21,22] for prolate nematic elastomers at temperatures where the main effects are due to the nematic order. Note, however, that the inequality $G_D < G_V$ can fail at temperatures close to the glass transition temperature ($T \sim T_g$); the consideration of glass transition effects is not a topic of the present paper. However, our model provides a true picture around the N−I transition, where the glass transition effects are rather small. For oblate systems ($l_\parallel < l_\perp$), we have the inequalities $G_D > G_V > G_G$, which are valid both for undeformed ($e_\parallel = e_\perp = 1$) and for deformed ($e_\parallel < 1 < e_\perp$) nematic elastomers. We have found no experimental data for G_G in prolate nematic elastomers and for G_D, G_V or G_G in oblate systems. Thus, our theory reproduces the experimental relation $G_D < G_V$ for prolate nematic elastomers and predicts additionally the inequalities $G_V < G_G$ (for prolate systems) and $G_D > G_V > G_G$ (for oblate systems). Note, that these above-found findings are universal, since they have been obtained now for polymer networks of arbitrary topology.

The next problem is to calculate the principal moduli as a function of the frequency and of the order parameter (or temperature). For this, it is necessary to know explicitly the eigenvalues λ_p and the viscoelastic parameters, $K_\parallel$, $K_\perp$, $\zeta_\parallel$, and $\zeta_\perp$ as functions of the order parameter *S*. These quantities are determined by the concrete structure of network strands and by the connectivity of the strands in the network. To fix the ideas, we consider in the next section a regular cubic polymer network built from freely jointed chains consisting of ellipsoidal particles.

4. Dynamic Modulus of a Regular Cubic Network Built from Anisotropic Chains

4.1. Model. We consider a network model topologically equivalent to a regular cubic structure, whose elementary cell contains a junction and three spacer chains (Figure 3). Such a cubic network model was used earlier for studying the dynamic properties of usual (isotropic) polymer networks.[39−41,43,45] The spacer chains between junctions are modeled here by chains consisting of the same number of freely jointed ellipsoidal particles with semiaxes *a* and $b = c$ (Figure 3). Such ellipsoidal particles imitate the mobility of Kuhn segments of real macromolecules.

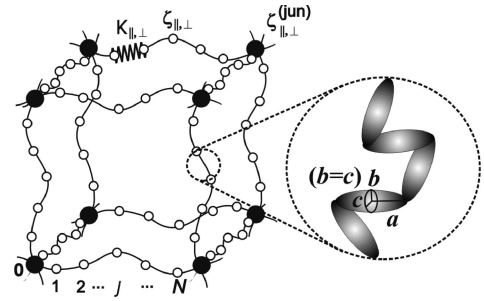

Figure 3. A topologically regular cubic network built from the chains consisting of freely jointed ellipsoidal particles. Network strands are divided into anisotropic Gaussian subchains. Friction coefficients of junction beads, $\zeta_{\parallel\perp}^{(jun)}$, include the friction of subchains attached to the cross-links, see text for details.

As described in section 2, we divide each spacer chain into equal subchains. Each subchain consists of *n* freely jointed ellipsoidal particles. The end-to-end distribution for long enough subchains ($n > 5$) becomes Gaussian. Each chain between junctions consists of the same number ($N + 1$) of subchains, which connect *N* spacer beads and two neighboring junctions. The persistence lengths for a freely jointed chain as a function of the order parameter (*S*) are given by:[8]

$$l_\parallel = l_0[1 + 2S], \quad l_\perp = l_0[1 - S] \quad (51)$$

where l_0 is the persistence length of a subchain in an isotropic state, $S = 0$.

The friction coefficients of each subchain, $\zeta_\parallel$ and $\zeta_\perp$, are the sum of friction coefficients for *n* ellipsoidal particles: $\zeta_{\parallel,\perp} = nkT/D_{\parallel,\perp}$, where $D_\parallel$ and $D_\perp$ are the average diffusion coefficients of the ellipsoidal particles along and perpendicular to the LC director. Here we have used Einstein's relation between friction and diffusion coefficients.[38] Furthermore, using eqs 20 and 21 of ref 34 for the diffusion coefficients $D_\parallel$ and $D_\perp$ in a system of ordered ellipsoidal particles, we obtain

$$\zeta_\parallel = \zeta_0\left(\frac{1 - RS}{1 + 2RS}\right)^{2/3}, \quad \text{and} \quad \zeta_\perp = \zeta_0\left(\frac{1 - RS}{1 + 2RS}\right)^{-1/3} \quad (52)$$

where ζ_0 is the friction coefficient of a subchain in an isotropic state and the parameter *R* is[34]

$$R = \frac{(a/b)^2 - 1}{(a/b)^2 + 2} \quad (53)$$

Recently,[37] it was shown by molecular dynamic simulations that the relations 52 and 53 are rather universal and hold not only for a system of *separate* ellipsoidal particles but also for polymer chains built from ellipsoidal particles, these relations staying unchanged when the bending rigidity of the chains is varied.[35−37]

Thus, Equations 5, 51−53 determine the viscoelastic parameters of subchains $K_\parallel$, $K_\perp$, $\zeta_\parallel$, and $\zeta_\perp$ as a function of the order parameter, *S*. Note, that *S* has here the physical meaning of an order parameter for the Kuhn segments of the network strands and can differ from the order parameter for mesogenic fragments which can be either in the main or in the side chains; in the

latter case the mesogenic fragments can be also attached to the backbone by a certain angle.

4.2. Eigenvalues and Characteristic Relaxation Times. Now, knowing the parameters $K_{||}$, $K_{\perp}$, $\zeta_{||}$, and $\zeta_{\perp}$ as a function of S, one can calculate the characteristic relaxation times, $\tau_D^{(0)}$, $\tau_G^{(0)}$ and $\tau_V^{(0)}$, as a function of S. Using eqs 51−53, one can rewrite eq 50 for $\tau_D^{(0)}$, $\tau_G^{(0)}$, and $\tau_V^{(0)}$ as follows:

$$\tau_D^{(0)} = \tau_G^{(0)} = 2\tau_0\left[\left(\frac{1 - RS}{1 + 2RS}\right)^{-2/3}(1 + 2S)^{-1} + \left(\frac{1 - RS}{1 + 2RS}\right)^{1/3}(1 - S)^{-1}\right]^{-1} \quad (54)$$

$$\tau_V^{(0)} = \tau_0\left[\left(\frac{1 - RS}{1 + 2RS}\right)^{-1/3}(1 - S)\right] \quad (55)$$

where τ_0 is the elementary relaxation time of a subchain in the isotropic state:

$$\tau_0 = \frac{\zeta_0 l_0 L}{3kT} \quad (56)$$

Now, one can estimate the characteristic values of the relaxation times for LC-polymer networks as compared with those for usual rubbers. The length of the subchain L, whose end-to-end distribution becomes Gaussian, is proportional to the persistence length of the chain, l_0: $L = nl_0$, with n being of the order of 5. Thus, we can rewrite eq 56 in the following form

$$\tau_0 = \xi l_0^3 n^2/3kT \quad (57)$$

where $\xi = \zeta_0/L$ is the linear density of friction along the polymer chain. We recall that LC-networks contain in their strands rigid and long mesogenic fragments. Therefore, both the parameters ξ and l_0 should be larger for LC-networks as compared with those for usual rubbers built from flexible chains. For side-chain macromolecules, the subchains include the friction parameters not only from the backbone but also from the side groups, so that ξ can be *much* greater for LC-networks as compared to the ξ value for usual rubbers. Moreover, the effective persistence length, l_0, of macromolecules bearing massive mesogenic groups in their side chains is expected to be also *much* greater than l_0 for usual rubbers due to the steric repulsion of the mesogenic groups in the side chains. As a result, due to the strong factor $\tau_0 \sim \xi l_0^3$ in eq 57 the characteristic relaxation times for the LC-network should be much larger than those for usual rubbers. We note that this conclusion is confirmed by the experiments[15,16,21−23] which show the characteristic relaxation times for LC-networks to be even 4 orders larger than the characteristic relaxation times for usual rubbers, see, e.g., page 320 of ref 16.

Anisotropic nematic elastomers are characterized by the differences in the values of the relaxation times for different geometries under shear, as it was found experimentally.[16,22] The difference between the values $\tau_V^{(0)}$ and $\tau_D^{(0)}$ ($\tau_D^{(0)} = \tau_G^{(0)}$) also follows from our theory. Using eqs 54 and 55, we have plotted in Figure 4 the ratio $\tau_D^{(0)}/\tau_V^{(0)}$ as a function of S for different ratios of the semiaxes of the ellipsoidal particles, a/b. One can see that $\tau_D^{(0)} > \tau_V^{(0)}$ at any values, $0 < S < 1$ and $a/b \geq 1$.

The inequality $\tau_D^{(0)} > \tau_V^{(0)}$ is confirmed experimentally, see, e.g., Figure 10 of ref 22. However, the difference between $\tau_V^{(0)}$ and $\tau_D^{(0)}$ turns out to be rather small. The difference between $\tau_D^{(0)}$ and $\tau_V^{(0)}$ increases with increasing order parameter. The maximal difference between $\tau_D^{(0)}$ and $\tau_V^{(0)}$ is $\tau_D^{(0)}/\tau_V^{(0)} = 2$, i.e. not large, see Figure 4. This means that the frequency dependences $G'(\omega)$ and $G''(\omega)$ for the D-geometry ($\mathbf{n} \| \mathbf{v}$) should be slightly shifted to lower frequencies as compared with these dependences for the V-geometry ($\mathbf{n} \perp \mathbf{v}$). This fact is visible in experiment: one can see from Figures 8−11 of ref 16 that the frequency

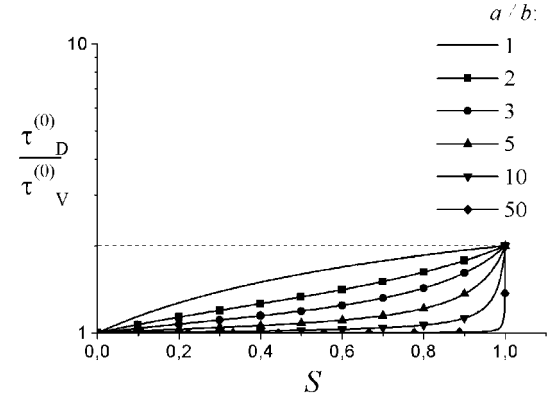

Figure 4. Ratio, $\tau_D^{(0)}/\tau_V^{(0)}$, ($\tau_G^{(0)} = \tau_D^{(0)}$) as a function of the order parameter S at different ratios of semiaxes of the ellipsoidal particles, a/b.

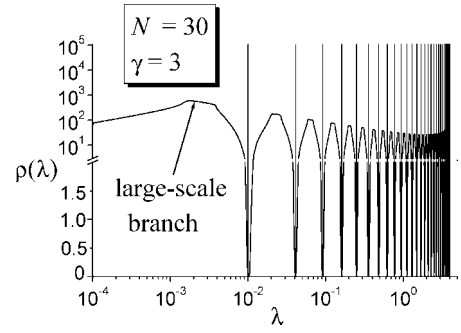

Figure 5. Spectral density, $\rho(\lambda)$, for a regular cubic network with $N = 30$ and $\gamma = 3$.

domain where $G'(\omega) = G''(\omega) \sim \omega^{1/2}$ for D-geometry ($\mathbf{n} \| \mathbf{v}$) is shifted to lower frequencies as compared with this domain for the V-geometry ($\mathbf{n} \perp \mathbf{v}$), this shift being rather small in accordance with our theory.

In order to calculate the frequency dependences of the principal moduli, it is necessary to know the eigenvalues λ_p of the network. For this, we use the results obtained recently[45] for the regular cubic network. It was found that the eigenvalues belong to two types. The first type, $\lambda_p^{(a)}$, corresponds to Rouse modes whose network junctions remain immobile:[45]

$$\lambda_p^{(a)} = 4\sin^2(\varphi_p/2) = 2(1 - \cos\varphi_p) \quad (58)$$

with $\varphi_p = p\pi/(N + 1)$ and $p = 1,..., N$. Each eigenvalue $\lambda_p^{(a)}$ appears twice.[45] The second kind of eigenvalues $\lambda^{(b)}$ corresponds to characteristic motions in which the network junctions move. The eigenvalues of the second kind are characterized (for an infinite network) by a continuous spectrum. Expression for the spectral density, $\rho(\lambda)$, is given by eq 46 of ref 45 where the parameters s and σ correspond in our notation to the number of beads between junctions ($s \equiv N$) and to the ratio between the friction coefficients of a network junction and a spacer bead ($\sigma \equiv \gamma = \zeta_\alpha^{(jun)}/\zeta_\alpha$). According to our model, γ is the number of chains intersecting at cross-link points; i.e., $\gamma = 3$ for the cubic model. In Figure 5 we present the spectral density, $\rho(\lambda)$, for $\gamma = 3$ which is calculated using the results of ref 45. The vertical solid lines show the Rouse eigenvalues, $\lambda_p^{(a)}$, given by eq 58. The continuous lines illustrate the spectral density, $\rho(\lambda)$, which includes, first, a large-scale branch with small λ and, second, narrow branches located close to the discrete Rouse eigenvalues, $\lambda_p^{(a)}$, see Figure 5.

4.3. Frequency Dependences of the Principal Moduli. Using the eigenvalues $\lambda_p^{(a)}$ and the continuous part of the spectrum we rewrite eq 48 for $G_{D,V,G}^* = G'_{D,V,G} + iG''_{D,V,G}$ as follows (cf. with eqs 49a−49c):

$$\frac{G_D^*(\omega)}{\nu kT} = {e_\perp}^2\frac{l_0}{l_\parallel} + \frac{l_\perp}{3l_\parallel}\left[2\sum_{p=1}^{N}\frac{(\omega\tau_D^{(0)})^2 + 2i\lambda_p^{(a)}\omega\tau_D^{(0)}}{(2\lambda_p^{(a)})^2 + (\omega\tau_D^{(0)})^2} + \int_0^\infty d\lambda\ \rho(\lambda)\frac{(\omega\tau_D^{(0)})^2 + 2i\lambda\omega\tau_D^{(0)}}{(2\lambda)^2 + (\omega\tau_D^{(0)})^2}\right] \quad (59a)$$

$$\frac{G_V^*(\omega)}{\nu kT} = {e_\perp}^2\frac{l_0}{l_\perp} + \frac{1}{3}\left[2\sum_{p=1}^{N}\frac{(\omega\tau_V^{(0)})^2 + 2i\lambda_p^{(a)}\omega\tau_V^{(0)}}{(2\lambda_p^{(a)})^2 + (\omega\tau_V^{(0)})^2} + \int_0^\infty d\lambda\ \rho(\lambda)\frac{(\omega\tau_V^{(0)})^2 + 2i\lambda\omega\tau_V^{(0)}}{(2\lambda)^2 + (\omega\tau_V^{(0)})^2}\right] \quad (59b)$$

$$\frac{G_G^*(\omega)}{\nu kT} = {e_\parallel}^2\frac{l_0}{l_\perp} + \frac{l_\parallel}{3l_\perp}\left[2\sum_{p=1}^{N-1}\frac{(\omega\tau_G^{(0)})^2 + 2i\lambda_p^{(a)}\omega\tau_G^{(0)}}{(2\lambda_p^{(a)})^2 + (\omega\tau_G^{(0)})^2} + \int_0^\infty d\lambda\ \rho(\lambda)\frac{(\omega\tau_G^{(0)})^2 + 2i\lambda\omega\tau_G^{(0)}}{(2\lambda)^2 + (\omega\tau_G^{(0)})^2}\right] \quad (59c)$$

The evaluation of each modulus implies now the numerical integration of functions which depend on $\rho(\lambda)$.

We present the results of the numerical evaluation of all the components of the dynamic moduli $G^*_{D,V,G}(\omega)$ in parts a and b of Figure 6 for $S = 0.3$ and 0.5, respectively. For simplicity, we consider a situation in which the sample is placed between two hard planes and does not stretch during the ordering ($e_\parallel = e_\perp = 1$), as in dynamic mechanical experiments.[15,16,21,22] The dashed lines in parts a and b of Figures 6 show the storage and loss moduli for an isotropic network.

The frequency behavior of $G^*_{D,V,G}(\omega)$ in parts a and b of Figure 6 is very similar to that obtained in experiments.[15,16,21,22] At low frequencies, the dynamic moduli demonstrate the hydrodynamic behavior ($G'_{D,V,G}(\omega) = G^{(eq)}_{D,V,G} = \text{const}$ and $G''_{D,V,G}(\omega) \sim \omega$, where $G^{(eq)}_{D,V,G}$ are the equilibrium moduli). After this domain there is a broad region with Rouse-like behavior $G'_{D,V,G} \cong G''_{D,V,G} \sim \omega^{1/2}$ due to the Rouse eigenvalues given by Equation 58. At higher frequencies the storage modulus has a final plateau and the storage modulus has a maximum. For all frequencies, the inequalities, $G'_D(\omega) < G'_V(\omega) < G'_G(\omega)$ and $G''_D(\omega) < G''_V(\omega) < G''_G(\omega)$, hold. The larger is the order parameter, the larger is the difference between G^*_D, G^*_V and G^*_G. We recall here that the inequalities $G'_D < G'_V$ and $G''_D < G''_V$ are visible also in experiment.[15,16,22]

As for isotropic networks,[39−45] we find here a simplified way for calculating $G^*_{D,V,G}(\omega)$ for ordered networks. It consists in the replacement of all complex branches of the relaxation spectrum by only (i) intrachain Rouse modes for all chains with immobile network junctions and (ii) the interchain (collective) mode for a coarse-grained (renormalized) network.[39−45] This procedure is based on the fact that the continuous spectrum $\rho(\lambda)$ includes N narrow branches which are localized close to the N Rouse eigenvalues, $\lambda_p^{(a)}$, Figure 5. These N narrow branches together with the exact Rouse modes $\lambda_p^{(a)}$ provide the eigenvalues for all chains between immobile junctions. Moreover, the continuous spectrum $\rho(\lambda)$ includes the large-scale branch with small λ (Figure 5); the eigenvalues of this branch are well approximated by those of a renormalized network which contains only the junctions connected by springs with an effective elasticity constant $K_\alpha^{(\text{eff})} = K_\alpha/(N+1)$ and in which the effective friction coefficient $\zeta_\alpha^{(\text{eff})}$ of each junction is the sum of all semichains coupled to this junction: $\zeta_\alpha^{(\text{eff})} = \zeta_\alpha^{(\text{jun})} + 3N\zeta_\alpha$.

The solid lines in Figures 7a and 7b show the exact frequency dependences for $G'_{D,V,G} - G^{(eq)}_{D,V,G}$ and for $G''_{D,V,G}$, respectively. The contributions from the intrachain (Rouse) modes and from the mode of a renormalized network are shown by dashed lines. It can be seen that the exact frequency dependences of the moduli are well approximated for $\tau_E^{-1} < \omega < \tau_0^{-1}$ by the intrachain Rouse-like modes which leads to the behavior $G'_{D,V,G} \cong G''_{D,V,G} \sim \omega^{1/2}$; at $\omega < \tau_E^{-1}$ the exact curves are mainly described by the collective interchain mode which leads to another power-type frequency behavior, namely $G'_{D,V,G} - G^{(eq)}_{D,V,G} \sim \omega^{3/2}$ and $G''_{D,V,G} \sim \omega$ at $\omega < \tau_E^{-1}$ (cf. with refs 39−45).

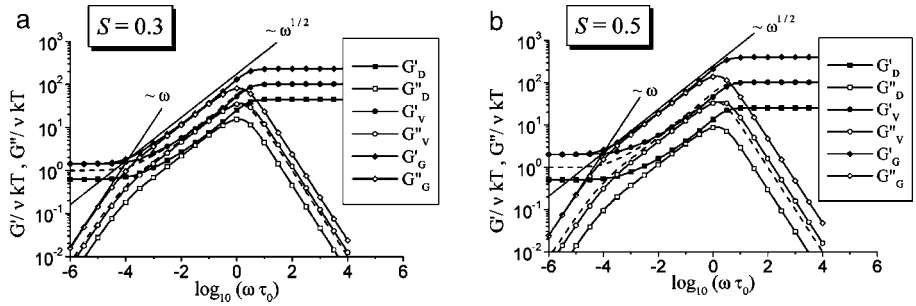

Figure 6. (a) Reduced storage, G', and loss, G'', moduli as functions of the reduced frequency, $\omega\tau_0$, for isotropic network (dashed lines) and for D, V, G geometries applied to an ordered nematic elastomer with $S = 0.3$ (solid lines). A regular cubic network model is used (Figure 3), $N = 100$, $\gamma = 3$, $a/b = 2$, $e_\parallel = e_\perp = 1$. (b) Same as Figure 6a, but for $S = 0.5$.

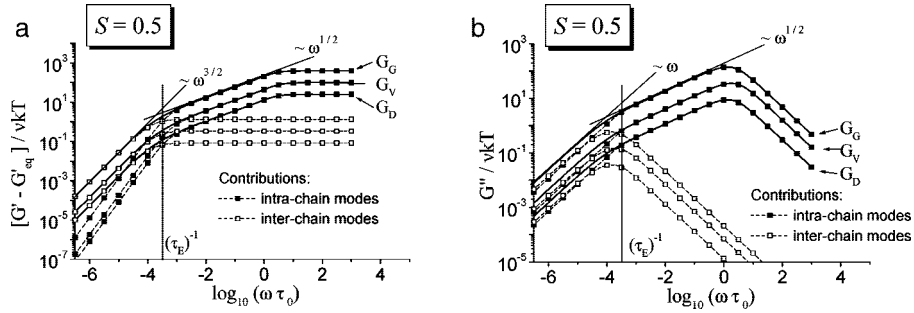

Figure 7. (a) Frequency dependences of the relaxation part of the storage moduli, $G'_{D,V,G}(\omega) - G^{(eq)}_{D,V,G}$, for an ordered nematic elastomer (solid lines). Contributions of intrachain (Rouse) and interchain (collective) modes are given by dashed lines with symbols. A regular cubic network model is used (Figure 3), $S = 0.5$, $N = 100$, $\gamma = 3$, $a/b = 2$, $e_\parallel = e_\perp = 1$. (b) Same as Figure 7a, but for the loss moduli, $G''_{D,V,G}(\omega)$.

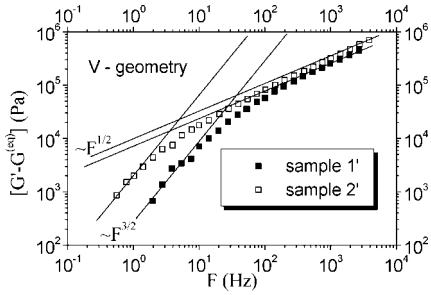

Figure 8. Frequency dependences of $G'_V - G'^{(eq)}_V$ reproduced from Figures 5 and 6 of ref 22 (for samples **2′** and **1′**) by subtraction of the values $G'^{(eq)}_V = 19.66kPa$ and $G'^{(eq)}_V = 60.77kPa$ (for samples **2′** and **1′**, respectively) from the values of G'_V given in ref 22.

In fact, parts a and b of Figure 7 illustrate the possibility of the separate use of the intra- and interchain modes. This result provides a simplified way for studying in the future the effects of the complex structure of network strands on the dynamics of nematic elastomers (e.g., the bending rigidity of chains, main- or side-chain macromolecules, etc.). First, one can simply calculate the eigenvalues of separate chains with immobile junctions (taking the local structure of network strands explicitly into account) and, second, calculate the large-scale eigenvalues for the corresponding renormalized Gaussian network. Here we use the fact that chain fragments of arbitrary structure obey Gaussian statistics when they are long enough.[8]

One of the interesting results obtained here is the power-low behavior, $G'_{D,V,G} - G'^{(eq)}_{D,V,G} \sim \omega^{3/2}$ at $\omega < \tau_E^{-1}$. This behavior was also found in theoretical works devoted to isotropic networks.[39,40,45] We note, however, that experimental works do not discuss usually the frequency behavior of G' around the low-frequency plateau, $G'^{(eq)}$, in the hydrodynamic regime $\omega < \tau_E^{-1}$. The problem to see experimentally the term $\sim\omega^{3/2}$ in the hydrodynamic regime consists in the fact that the quantities G' and $G'^{(eq)}$ are close to each other in this frequency domain, so that the errors of the difference $G' - G'^{(eq)}$ can be of the same order as the quantity $G' - G'^{(eq)}$ itself. Thus, to see the term $G' - G'^{(eq)} \sim \omega^{3/2}$ experimentally, it is necessary, first, to plot the quantity $\log_{10}[G' - G'^{(eq)}]$ instead of $\log_{10}[G']$, and, second, to use equipment which is precise enough to obtain the value $G' - G'^{(eq)}$.

Another problem is related with the polydispersity of network strands. The power-law $G' - G'^{(eq)} \sim \omega^{3/2}$ takes place only for regular networks built from identical chains. However, the polydispersity of network strands, which takes place in real cross-linked systems, can lead to a more rapid power-law behavior $G' - G'^{(eq)} \sim \omega^2$ at $\omega < \tau_E^{-1}$, see, e.g., eq 37 of ref 41. Thus, one can conclude that the quantity $G' - G'^{(eq)}$ should demonstrate more rapid frequency behavior at $\omega < \tau_E^{-1}$ as compared with the dependence $G' - G'^{(eq)} \sim \omega^{1/2}$ at $\omega > \tau_E^{-1}$.

To check these theoretical findings we have replotted in Figure 8 the experimental data given by Figures 5 and 6 of ref 22 for two nematic elastomers (samples **2′** and **1′**, respectively). Samples **2′** and **1′** were synthesized at the Institut für Makromolekulare Chemie in Freiburg. These samples are based on poly[oxi(methilsilylene)]'s network; they are different only in their cross-linkers; see ref 22 for details.

Instead of the quantities G'_V given in ref 22 for the V-geometry we have plotted in Figure 8 the values $G'_V - G'^{(eq)}_V$ by subtracting the values $G'^{(eq)}_V \approx 19.66$ kPa and $G'^{(eq)}_V \approx 60.77$ kPa (for samples **2′** and **1′**, respectively) from the values G'_V of ref 22 The value of τ_E has been found to be $\sim 5 \times 10^{-2}$ s (sample **2′**) and $\sim 4 \times 10^{-3}$ s (sample **1′**), see p 374 of ref 22. Using these values of τ_E, one can see from Figure 8 that the experimental data replotted in such a way confirm the theoretical findings obtained above: the frequency dependence $G' - G'^{(eq)}$ demonstrate more rapid

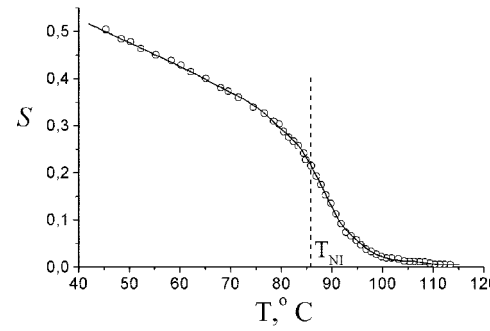

Figure 9. Order parameter S as a function of the temperature for a side-chain nematic elastomer based on poly[oxi(methilsilylene)]'s network. Reproduced with permission from Figure 2b of ref 10. Copyright 1994 Wiley. $T_{NI} \approx 359$ K (or $T_{NI} \approx 86$ °C), see Table 1 of ref 10.

behavior ($\sim f^n$, with $n > 1$) at $f < \tau_E^{-1}$ as compared with this dependence ($\sim f^{1/2}$) at $f > \tau_E^{-1}$. The frequency behavior of $G'(\omega)$ around the low-frequency plateau can be analyzed more carefully in the future.

Here we note that the frequency range of the power law $G' - G'^{(eq)} \sim f^n$ (with $n > 1$), can be extended practically in at least two ways. First, one can rely on instrumentation precise enough to measure the quantity $G' - G'^{(eq)}$ in the low frequency region where the value of $G' - G'^{(eq)}$ is very small. Second, one may synthesize a heterogeneous network system with a broad distribution of contour lengths of network strands. In this case, the frequency domain with a Rouse-like behavior should be shorter due to strong heterogeneity but the frequency range of the power law $G' - G'^{(eq)} \sim f^n$ (with $n > 1$) is expected to be broader.

4.4. Temperature Dependences of the Principal Moduli at Fixed Frequency. One of the interesting characteristics to be studied experimentally is the temperature dependence of the principal moduli. The temperature dependence of the principal moduli is determined by the temperature dependence of the order parameter, $S = S(T)$. Here we recall that the dependence $S = S(T)$ for monodomain nematic elastomers has a specific character due to the sample preparation.[9−12,16,22] Monodomain samples are produced by stretching the sample during the synthesis; the mechanical stresses to be used should be much greater than the mechanical critical point, $\sigma > \sigma_{cp}$.[9−12,16,22] As a result, a produced monodomain sample turns out to be in a supercritical state which is characterized by a continuous increase of the order parameter with decreasing temperature. Such a continuous dependence $S = S(T)$ distinguishes the monodomain nematic elastomers from the low-molecular-weight LCs which show a jump of the order parameter, S, at the N−I phase transition.[9]

In order to calculate the temperature dependences of the principal moduli, we use the *experimental* dependence $S = S(T)$ given by Figure 2b of ref 10, which is reproduced here in Figure 9. We note that in the supercritical state, the nematic and the isotropic phases cannot be differentiated anymore and, therefore, the N−I phase transition temperature, $T_{NI} \approx 359$ K (or $T_{NI} \approx 86$ °C), determined in ref.[10] (Table 1) by differential scanning calorimetry (DSC) is a pseudo N−I phase transition temperature, see also the discussion on pages 371 and 372 of ref 22.

Parts a−d of Figure 10 show temperature dependence of the storage moduli $G'_{D,V,G}$, which have been calculated using the dependence $S = S(T)$ given in Figure 9. The different panels a−d correspond to different values of the reduced frequency, $\omega\tau_E$. For the calculations eqs 59a−59c have been used, where the parameters $l_{\parallel,\perp}$, $\tau_D^{(0)}$, $\tau_G^{(0)}$, and $\tau_V^{(0)}$ change with S according to eqs 51−56. The elongation ratios $e_\parallel$ and $e_\perp$ are chosen for two types of boundary conditions. The solid lines in Figures 10a-

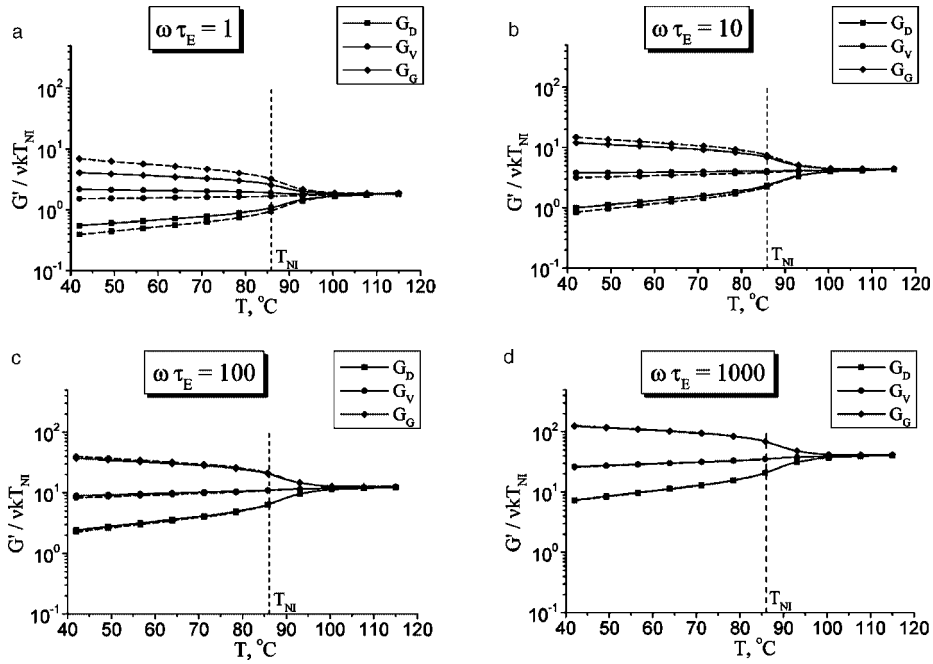

Figure 10. Reduced storage moduli, $G'_{D,V,G}$, as functions of temperature T for a nematic elastomer with fixed boundaries ($e_{||} = e_{\perp} = 1$, solid lines) and for a stress-free nematic elastomer which is stretched along the LC director (dashed lines). A regular cubic network model is used (Figure 3), $N = 100$, $\gamma = 3$, $a/b = 2$. The different panels illustrate the results for different values of the parameter $\omega\tau_E$: (a) $\omega\tau_E = 1$, (b) $\omega\tau_E = 10$, (c) $\omega\tau_E = 100$, and (d) $\omega\tau_E = 1000$.

10d correspond to the case in which a sample is placed between two hard plates and does not change its shape during ordering ($e_{||} = e_{\perp} = 1$). This situation was realized in experiments.[15,16,21,22] The dashed lines in parts a−d of Figure 10 illustrate the results for a nematic elastomer with free boundaries, when it is stretched along the director during ordering as it was realized in experiment.[22] The elongation ratio, $e_{||}$, is determined in the last case by the well-known condition,[3−8,25,26]

$$e_{||} = (l_{||}/l_{\perp})^{1/3} \tag{59}$$

and $e_{\perp}$ changes in accordance with the condition of constant volume for elastomers, $e_{\perp} = 1/\sqrt{e_{||}}$.

One can see from parts a−d of Figure 10 that the mechanical constrains affect rather weakly the temperature dependences of the moduli: the differences between the moduli for a sample with fixed and free boundaries are rather small. The stretching of the network with free boundaries (dashed lines in Figure 10a−d) leads to larger differences between G'_D, G'_V and G'_D as compared with these dependences for a network with fixed boundaries, due to the additional anisotropy of the network with free boundaries caused by its deformation. However, the changes in the values of G'_D, G'_V, and G'_D, caused by the boundary conditions is not significant, as can be seen from Figures 10a-10d. This fact was also found experimentally[16,22] by measuring and comparing the values of the moduli for a sample placed between hard plates in a rheometer and for a preliminary heated (and spontaneously stretched) elastomer placed then between the plates.

The temperature dependences, $G'_{D,V,G} = G'_{D,V,G}(T)$, for elastomers with both free and fixed boundaries demonstrate the following behavior. At $T > T_{NI}$ we have $G'_D = G'_V = G'_G$, and due to the Boltzmann factor ($\sim\nu kT$) the values of $G'_{D,V,G}$ decrease when the temperature decreases. Around T_{NI}, the storage moduli, G'_D and G'_G, have singularities: G'_D decreases greatly due to the prefactor $l_{\perp}/l_{||}$ in the frequency term in eq 59a, whereas G'_G increases greatly due to the opposite prefactor $l_{||}/l_{\perp}$ in eq 59c. However, G'_V has no such prefactors (see eq 59b) and changes rather weakly at $T = T_{NI}$, see Figure 10a−d. With further decreasing temperatures $T < T_{NI}$, G'_D, and G'_V decrease, whereas G'_G increases slowly; see Figure 10a−d.

The results for the D- and V-geometries obtained above are in a fine agreement with the experimental data for all existing monodomain side-chain nematic elastomers.[15,16,21,22] There is only one remark which is related to the glass transition. In real elastomers glass transition effects become very strong at low temperatures, and both G'_D and G'_V start to increase strongly when the temperature decreases.[15,16,21,22] At high frequencies the glass transition effects are rather strong even at $T \cong T_{NI}$. Our theory does not consider glass transition effects; it gives, however, an absolutely true picture for G'_D and G'_V around T_{NI}, where the glass transition effects are weak and the main effects are due to the nematic-like interactions.[15,16,21,22]

It should be pointed out that the G-geometry was not realized in the recent experiments and we have found no such realizations in literature. Perhaps, this is caused by difficulties (or special problems) related to the preparation of a LC film with the director lying perpendicular to the film. Thus, our results for $G'_G = G'_G(T)$ can be considered as a prediction of the theory and we hope that our findings will stimulate in future new dynamic mechanical experiments for nematic elastomers.

We conclude the paper by recalling that our model uses an approach in which the LC-director is immobile. Such approach works well enough at $\tau_E^{-1} < \omega < \tau_0^{-1}$, where the LC-director can be really considered as immobile, since the characteristic time of its rotation, τ_n, is of the same order as the longest relaxation time of the networks strands, $\tau_E \sim \tau_n$.[16,22] To consider the phenomenon at $\omega < \tau_E^{-1}$ one should take into account the rotations of the LC-director. Of course, these effects can be considered in further theories. However, a fine agreement of our approach with experimental data both at $\omega < \tau_E^{-1}$ and at $\tau_E^{-1} < \omega < \tau_0^{-1}$ allows one to expect that the effect of director rotation will not change dramatically the results of our theory. This conclusion is confirmed also by light scattering experiments[13] which have shown that the fluctuations

of the LC director in monodomain nematic elastomers are strongly suppressed by network elastic restoring torques. Moreover, in low-frequency limit, $\omega \ll \tau_E^{-1}$, the value of G' is close to the equilibrium value, $G^{(eq)}$, which is independent of any dynamic effects including the rotation of the director. Thus, the main effects of the director rotations are expected around $\omega \sim \tau_n^{-1} \sim \tau_E^{-1}$, where an interesting combination of network dynamics and the dynamics of the LC-director can appear.

Conclusions

We have proposed a microscopic theory for the dynamic mechanical properties of nematic elastomers. It is the first theory which takes explicitly into account the chain structure of network strands in nematic elastomers. We use an approach in which the fragments of polymer chains in LC state are considered to move on the background of an immobile LC director. We consider the chain dynamics on scales larger than a Kuhn segment. In this approach, a polymer chain is modeled as a sequence of Gaussian subchains with anisotropic values of their visco-elastic parameters with respect to the LC- director (modified Rouse model).

We have derived exact expressions for three principal dynamic moduli, G_D^*, G_V^*, and G_G^*, corresponding to the D, V, and G geometries of the mechanical shear (Figure 1), for rather arbitrary network structures built from anisotropic Gaussian chains. For prolate networks, the relations $G'_D < G'_V < G'_G$ and $G''_D < G''_V < G''_G$ hold, whereas for oblate systems the opposite inequalities are obeyed. These results are valid both for a stress-free network which can change its shape during ordering and for a network between fixed plates, when the shape of the network is kept unchanged by applying an appropriate external stress. We have found that the frequency dependence of the dynamic moduli, G_D^*, G_V^*, and G_G^*, is determined by the eigenvalues of an isotropic network structure of the same topology. It allows us to extend the results of previous works for conventional (isotropic) rubbers[39−45] to LC−polymer networks. From such a generalization we obtain the following rather general results for prolate nematic elastomers. **(1)** Around the temperature of the nematic−isotropic phase transition, G_D^* decreases and G_G^* increases greatly, whereas G_V^* has no such singularities. **(2)** The frequency dependences of the principal moduli show for $\omega < \tau_E^{-1}$ a hydrodynamic behavior ($G'_{D,V,G} = G^{(eq)}_{D,V,G} = \text{const}$ and $G''_{D,V,G} \sim \omega$, where $G^{(eq)}_{D,V,G}$ are the equilibrium moduli) and a Rouse-like behavior ($G'_{D,V,G} \cong G''_{D,V,G} \sim \omega^{1/2}$) for $\tau_E^{-1} < \omega < \tau_0^{-1}$. Here τ_0 and τ_E are the minimal and maximal relaxation times of the network strands. **(3)** The frequency dependences $G'_{D,V,G}(\omega)$ at $\omega < \tau_E^{-1}$ display a power-type behavior $G'_{D,V,G}(\omega) - G^{(eq)}_{D,V,G} \sim \omega^{\alpha}$, which is more rapid ($\alpha > 1$) than the Rouse-like behavior, $G'_{D,V,G} \cong G''_{D,V,G} \sim \omega^{1/2}$, at $\tau_E^{-1} < \omega < \tau_0^{-1}$. **(4)** The characteristic relaxation times for all modes, including τ_0 and τ_E, are shown to be much larger for LC-networks than the corresponding relaxation times for conventional rubbers. **(5)** The characteristic relaxation times for the V-geometry are slightly larger than those for the D- and G-geometries in the nematic state. **(6)** The boundary constraints (fixed or free boundaries of a sample) affect rather slightly the dynamic mechanical behavior of nematic elastomers. The results (1−6) have been illustrated here by using a regular cubic network model built from anisotropic Gaussian chains.

All the results (1−6) for the D- and V- geometries are in a fine agreement with the experimental data obtained for side-chain nematic elastomers in refs 15, 16, 21, and 22. The agreement of the results of our theory with the experimental data[15,16,21,22] demonstrates the great potential strength of the proposed microscopic approach for describing the dynamics of nematic elastomers. We note, however, that the Gaussian chain model used here cannot be applied to main-chain nematic elastomers existing at present,[23] since they show SmC-domains in their structures. At the same time, this model can be directly applied to side-chain nematic elastomers, since they do not demonstrate such heterogeneities in their structure.[15,16,21,22]

We conclude by noting that recent dynamic mechanical experiments have used only D- and V-geometries in their analysis; there are no experimental data in the literature for the G-geometry. Thus, our results for the G-geometry can be considered as a prediction of the theory, and we hope that our findings can stimulate in future new dynamic mechanical experiments for nematic elastomers.

Acknowledgment. We cordially thank Prof. A. Blumen and Prof. H. Brand for stimulating discussions and for reading the manuscript. It is a pleasure to thank Prof. H. Finkelmann and Prof. G. Heinrich for helpful discussions. The support of the Russian Foundation for Basic Research (Grant 08-03-00150), of INTAS (04-83-2912) and of the Deutsche Forschungsgemeinschaft is gratefully acknowledged.

References and Notes

(1) Jarry, J. P.; Monnerie, L. *Macromolecules* **1979**, *12*, 316–320.
(2) De Gennes, P. G. Weak nematic gels. In *Liquid Crystals of One- and Two-Dimensional Order*; Helfrich, W., Heppke, G., Eds.; Springer: Berlin, 1980; pp 231−237.
(3) Rusakov, V. V.; Shliomis, M. I. *J. Phys., Lett.* **1985**, *46*, L935−L943.
(4) Abramchuk, S. S.; Nyrkova, I. A.; Khokhlov, A. R. *Polym. Sci. (Russ.) Ser. A.* **1989**, *31*, 1759–1765.
(5) Warner, M.; Wang, X. J. *Macromolecules* **1991**, *24*, 4932–4931.
(6) Warner, M.; Bladon, P.; Terentjev, E. M. *J. Phys. II. Fr.* **1994**, *4*, 93–102.
(7) Warner, M.; Terentjev, E. M. *Prog. Polym. Sci.* **1996**, *21*, 853–891.
(8) Wang, X. J. *Prog. Polym. Sci.* **1997**, *22*, 735–764.
(9) Küpfer, J.; Finkelmann, H. *Macromol. Chem. Rapid Commun.* **1991**, *12*, 717–726.
(10) Disch, S.; Schmidt, C.; Finkelmann, H. *Macromol. Rapid Commun.* **1994**, *15*, 303–310.
(11) Brand, H.; Kawasaki, K. *Macromol. Rapid Commun.* **1994**, *15*, 251–257.
(12) Brand, H.; Pleiner, H. *Physica A.* **1994**, *208*, 359–372.
(13) Schönstein, M.; Stille, W.; Strobl, G. *Eur. Phys. J. E* **2001**, *5*, 511–517.
(14) Terentjev, E. M.; Warner, M. *Eur. Phys. J. E* **2001**, *4*, 343–353.
(15) Stein, P.; Aβfalg, N.; Finkelmann, H.; Martinoty, P. *Eur. Phys. J. E* **2001**, *4*, 255–262.
(16) Martinoty, P.; Stein, P.; Finkelmann, H.; Pleiner, H.; Brand, H. R. *Eur. Phys. J. E* **2004**, *14*, 311–321.
(17) Terentjev, E. M.; Warner, M. *Eur. Phys. J. E* **2004**, *14*, 323–327.
(18) Martinoty, P.; Stein, P.; Finkelmann, H.; Pleiner, H.; Brand, H. R. *Eur. Phys. J. E* **2004**, *14*, 329–332.
(19) Stenull, O.; Lubensky, T. C. *Eur. Phys. J. E* **2004**, *14*, 333–337.
(20) Martinoty, P.; Stein, P.; Finkelmann, H.; Pleiner, H.; Brand, H. R. *Eur. Phys. J. E* **2004**, *14*, 339–340.
(21) Brand, H. R.; Pleiner, H.; Martinoty, P. *Soft Matter* **2006**, *2*, 182–189.
(22) Rogez, D.; Francius, G.; Finkelmann, H.; Martinoty, P. *Eur. Phys. J. E* **2006**, *20*, 369–378.
(23) Rogez, D.; Brandt, H.; Finkelmann, H.; Martinoty, P. *Macromol. Chem. Phys.* **2006**, *207*, 735–745.
(24) Gotlib, Yu. Ya.; Torchinskii, I. A.; Toshchevikov, V. P. *Macromol. Theory Simul.* **2002**, *11*, 898–912.
(25) Toshchevikov, V. P. *Orientation order in densely cross-linked polymer networks: electro optical and relaxation characteristics. Ph.D. Thesis*; Institute of Macromolecular Compounds: Saint Petersburg, Russia, 2002; p 228.
(26) Gotlib, Yu. Ya.; Torchinskii, I. A.; Toshchevikov, V. P. *Macromol. Theory Simul.* **2004**, *13*, 303–317.
(27) Urayama, K. *Macromolecules* **2007**, *40*, 2277–2288.
(28) Gotlib, Yu. Ya. *Prog. Colloid Polym. Sci.* **1989**, *80*, 245–253.
(29) Darinskii, A. A.; Gotlib, Yu. Ya.; Lyulin, A. V.; Neelov, I. M. *Polym. Sci. USSR. Ser. A.* **1992**, *34*, 11–15.
(30) Darinskii, A.; Gotlib, Yu.; Lukyanov, M.; Lyulin, A.; Neelov, I. M. *Prog. Colloid Polym. Sci.* **1993**, *91*, 13–15.
(31) Gotlib, Yu.; Medvedev, G.; Fridrikh, S. *Macromol. Chem., Macromol. Symp* **1993**, *65*, 153–162.
(32) Long, D.; Morse, D. C. *J. Rheol.* **2002**, *46*, 49–92.
(33) Rouse, P. E. *J. Chem. Phys.* **1953**, *21*, 1272–1280.
(34) Hess, S.; Frenkel, D.; Allen, M. P. *Mol. Phys.* **1991**, *74*, 765–774.

(35) Bruggen, M. P. B.; Lekkerkerker, H. N. W.; Maret, G.; Dont, J.K. G. *Phys. Rev. E.* **1998**, *58*, 7668–7677.
(36) Löwen, H. *Phys. Rev. E.* **1999**, *59*, 1989–1995.
(37) Darinskii, A. A.; Zarembo, A.; Balabaev, N. K.; Neelov, I. M.; Sundholm, F. *Phys. Chem. Chem. Phys.* **2003**, *5*, 2410–2416.
(38) Doi, M.; Edwards, S. F. *The Theory of Polymer Dynamics*; Clarendon: Oxford, U.K., 1986; p 391.
(39) Gurtovenko, A. A.; Gotlib, Yu. Ya. *Macromolecules* **1998**, *31*, 5756–5770.
(40) Gurtovenko, A. A.; Gotlib, Yu. Ya. *Macromolecules* **2000**, *33*, 6578–6587.
(41) Gurtovenko, A. A.; Gotlib, Yu. Ya.; Kilian, H. G. *Macromol. Theory. Simul.* **2000**, *9*, 388–397.
(42) Satmarel, C.; Gurtovenko, A. A.; Blumen, A. *Macromolecules* **2003**, *36*, 486–494.
(43) Gurtovenko, A. A.; Blumen, A. *Adv. Polym. Sci.* **2005**, *182*, 171–282.
(44) Satmarel, C.; von Ferber, C.; Blumen, A. *J. Chem. Phys.* **2005**, *123*, 034907.1−034907.13.
(45) Toshchevikov, V. P.; Blumen, A.; Gotlib, Yu. Ya. *Macromol. Theory Simul.* **2007**, *16*, 359–377.
(46) Ferry, J. *Viscoelastic Properties of Polymers*, 3rd ed.; Wiley: New York, 1980; p 668.
(47) Larson, R. G. *The structure and rheology of complex fluids*; Oxford University Press: New York, 1999; p 663.

MA802757G